Cell Reports
Physical Science

CellPress
OPEN ACCESS

Article

Electrostatic interaction determines thermal conductivity anisotropy of Bi_2O_2Se

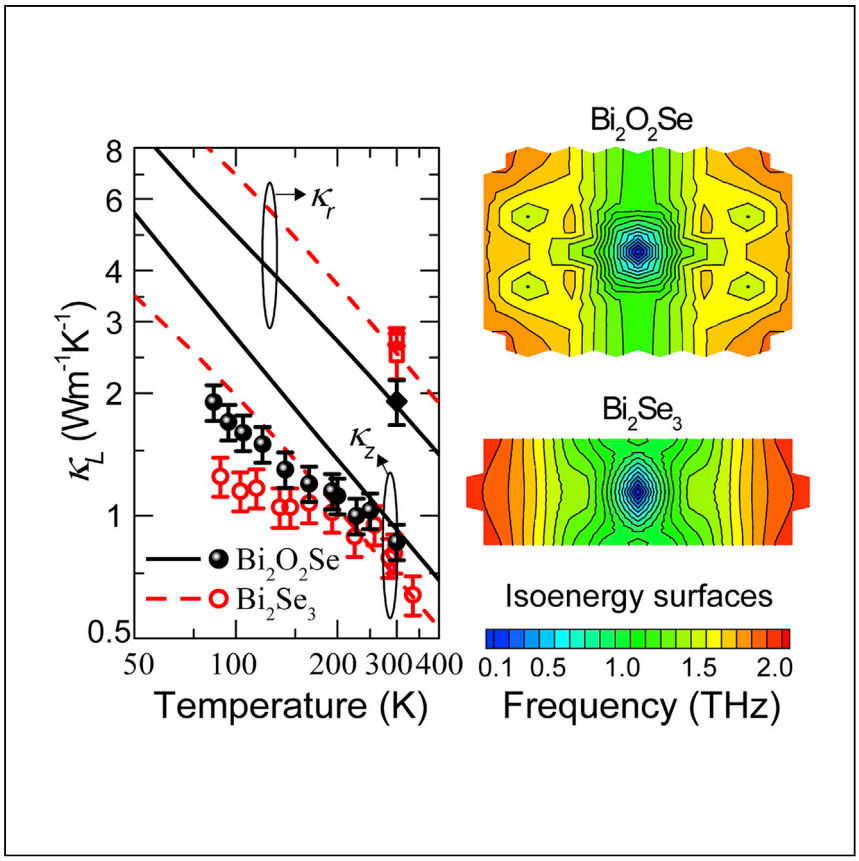

The alternating layers in Bi_2O_2Se are coupled by electrostatic forces rather than van der Waals interactions that commonly exist in layered materials. Guo et al. show that the relatively stronger electrostatic interactions result in weakened phonon focusing and, thus, substantially smaller thermal anisotropy in Bi_2O_2Se compared with Bi_2Se_3.

Ruiqiang Guo, Puqing Jiang, Teng Tu, Sangyeop Lee, Bo Sun, Hailin Peng, Ronggui Yang

ronggui@hust.edu.cn

Highlights

Determination of thermal anisotropy of Bi_2O_2Se by experiments and calculations

Substantially smaller thermal anisotropy in Bi_2O_2Se compared with Bi_2Se_3

Weakened phonon focusing along the in-plane directions in Bi_2O_2Se

Dominant influence of electrostatic interaction on the thermal anisotropy of Bi_2O_2Se

Guo et al., Cell Reports Physical Science 2, 100624
November 17, 2021 © 2021
https://doi.org/10.1016/j.xcrp.2021.100624

Please cite this article in press as: Guo et al., Electrostatic interaction determines thermal conductivity anisotropy of Bi_2O_2Se, Cell Reports Physical Science (2021), https://doi.org/10.1016/j.xcrp.2021.100624

Cell Reports
Physical Science

Article

Electrostatic interaction determines thermal conductivity anisotropy of Bi_2O_2Se

Ruiqiang Guo,[1,6] Puqing Jiang,[2,6] Teng Tu,[3] Sangyeop Lee,[4] Bo Sun,[5] Hailin Peng,[3] and Ronggui Yang[2,7,*]

SUMMARY

The air-stable layered semiconductor Bi_2O_2Se has recently attracted extensive interest because of its potential application in electronics, optoelectronics, ferroelectrics, and thermoelectrics. For many of these applications, thermal transport in Bi_2O_2Se is of great importance, but a complete understanding of the process remains elusive. Here, we perform a combined experimental and theoretical study of the anisotropic thermal conductivity of single-crystalline Bi_2O_2Se in comparison with Bi_2Se_3. Bi_2O_2Se exhibits relatively higher through-plane thermal conductivity but lower in-plane thermal conductivity, resulting in substantially smaller thermal anisotropy. This behavior originates from the stronger interlayer electrostatic interaction in Bi_2O_2Se compared with the typical van der Waals coupling in layered materials, making the phonon isoenergy surfaces less anisotropic and, thus, weakening phonon focusing in the in-plane directions. Our study advances the fundamental understanding of thermal anisotropy in layered materials with various interlayer interactions and will facilitate application of Bi_2O_2Se in electronics and thermoelectrics.

INTRODUCTION

As a typical bismuth oxychalcogenide material, Bi_2O_2Se has recently drawn great interest because of its high mobility, tunable electronic band gap, and excellent air stability, which make it a promising next-generation semiconductor for electronics, optoelectronics, ferroelectrics, and thermoelectrics.[1–12] The remarkable properties of Bi_2O_2Se benefit from its mixed-anion chemical bonding and layered structures with alternating tetragonal oxide (Bi_2O_2) and chalcogenide (Se) layers. Extensive efforts have been devoted to exploring its electrical properties.[1–3,10,11,12] For instance, ultrahigh Hall mobility at low temperatures and thickness-dependent band gaps have been observed.[1,12] By applying external strain and engineering defects, the electrical properties can be modulated significantly.[11] In contrast, thermal properties that are crucial in many applications, from the thermal management of electronics to thermoelectric energy conversion, have rarely been studied. Polycrystalline Bi_2O_2Se has been measured to have low thermal conductivity, with values varying from 0.35–1.7 W m^{-1} K^{-1} at 300 K.[5,7,8,13–19] This wide range of values may be attributed to different sample qualities and/or even the accuracy of measurement techniques.

Layered materials can possess high thermal anisotropy (defined as the ratio between in-plane and through-plane thermal conductivity) and extremely low through-plane thermal conductivity that is not attainable in isotropic materials. Graphite, a

[1]Thermal Science Research Center, Shandong Institute of Advanced Technology, Jinan, Shandong Province 250103, China

[2]School of Energy and Power Engineering, Huazhong University of Science and Technology, Wuhan, Hubei 430074, China

[3]Center for Nanochemistry, Beijing National Laboratory for Molecular Sciences, College of Chemistry and Molecular Engineering, Peking University, Beijing 100871, China

[4]Department of Mechanical Engineering and Materials Sciences, University of Pittsburgh, Pittsburgh, PA 15261, USA

[5]Tsinghua-Berkeley Shenzhen Institute and Guangdong Provincial Key Laboratory of Thermal Management Engineering and Materials, TSIGS, Tsinghua University, Shenzhen 518055, China

[6]These authors contributed equally

[7]Lead contact

*Correspondence: ronggui@hust.edu.cn

https://doi.org/10.1016/j.xcrp.2021.100624

Please cite this article in press as: Guo et al., Electrostatic interaction determines thermal conductivity anisotropy of Bi_2O_2Se, Cell Reports Physical Science (2021), https://doi.org/10.1016/j.xcrp.2021.100624

common layered material, has received extensive attention because of its extreme thermal anisotropy, with a high in-plane thermal conductivity of 2,000 W m^{-1} K^{-1} but only 6 W m^{-1} K^{-1} in the through-plane direction.[20] SnSe has been reported to possess a record-high thermoelectric figure of merit, largely because of the exceptionally low thermal conductivity in the through-plane direction.[21] The layers in these layered materials are typically stacked together by van der Waals interactions. Bi_2O_2Se is synthesized by partially replacing Se atoms with O atoms in its parent compound Bi_2Se_3, a widely studied Bi-based van der Waals layered thermoelectric material with low thermal conductivity in the through-plane direction. Instead of van der Waals interactions in Bi_2Se_3, a relatively stronger electrostatic force couples the alternating layers in Bi_2O_2Se. How this interlayer interaction difference affects thermal anisotropy remains unexplored.

The thermal anisotropy of layered materials is often determined by the phonon focusing effect.[22–24] Specifically, anisotropic bonding in layered materials results in non-spherical isoenergy surfaces in the Brillouin zone. Because the group velocity vector is normal to the isoenergy surface, the non-spherical isoenergy surfaces produce a larger decomposition of the group velocity vector in in-plane directions compared with the through-plane direction, as observed for MoS_2 and WS_2.[24] Compared with van der Waals interaction, the stronger electrostatic interlayer interaction is expected to produce smaller bonding anisotropy, resulting in weaker phonon focusing and smaller thermal anisotropy. A deep understanding of the underlying mechanisms governing the thermal anisotropy in layered materials that are coupled by different forces will help to further manipulate thermal properties, such as by constructing heterostructures. For instance, an extremely low thermal conductivity of 0.1 W $m^{-1}K^{-1}$ was achieved in the superlattice $Bi_4O_4SeCl_2$ by combining the longitudinal acoustic (LA) phonon softening in BiOCl and transverse acoustic (TA) softening and anharmonicity in Bi_2O_2Se.[19] Also, controlling coherent phonon transport using heterostructures stacked by atomically thin layers has been demonstrated to be an effective way to dramatically change thermal anisotropy.[24]

In this work, we conduct a comprehensive study on the anisotropic thermal conductivity of bulk single-crystalline Bi_2O_2Se in comparison with Bi_2Se_3 by combining the time-domain thermoreflectance (TDTR) measurements and *ab initio* phonon Boltzmann transport calculations. We reveal a much smaller thermal anisotropy in Bi_2O_2Se relative to Bi_2Se_3, originating from the relatively stronger interlayer electrostatic interaction in Bi_2O_2Se compared with the typical van der Waals coupling in Bi_2Se_3. The stronger interlayer bonding strength makes the phonon isoenergy surfaces less anisotropic and weakens phonon focusing in the in-plane directions. Our study advances the fundamental understanding of thermal anisotropy in layered materials with various interlayer interactions and will facilitate application of Bi_2O_2Se in electronics and thermoelectrics.

RESULTS AND DISCUSSION

Crystal structure and lattice dynamics

Figure 1 shows the layered structures of Bi_2O_2Se and Bi_2Se_3. Bi_2Se_3 is a relatively well-studied thermoelectric material and has a rhombohedral structure (space group $R\bar{3}m$), consisting of Se1-Bi-Se2-Bi-Se1 quintuple layers stacked by van der Waals interactions. Instead of van der Waals interactions, Bi_2O_2Se crystallizes in a tetragonal structure (space group *I4/mmm*), with the Bi_2O_2 and Se layers held together by weak electrostatic interaction. Because of the different crystal structures, Bi_2O_2Se and Bi_2Se_3 possess markedly different phonon dispersion and density of states (DOS),

Please cite this article in press as: Guo et al., Electrostatic interaction determines thermal conductivity anisotropy of Bi_2O_2Se, Cell Reports Physical Science (2021), https://doi.org/10.1016/j.xcrp.2021.100624

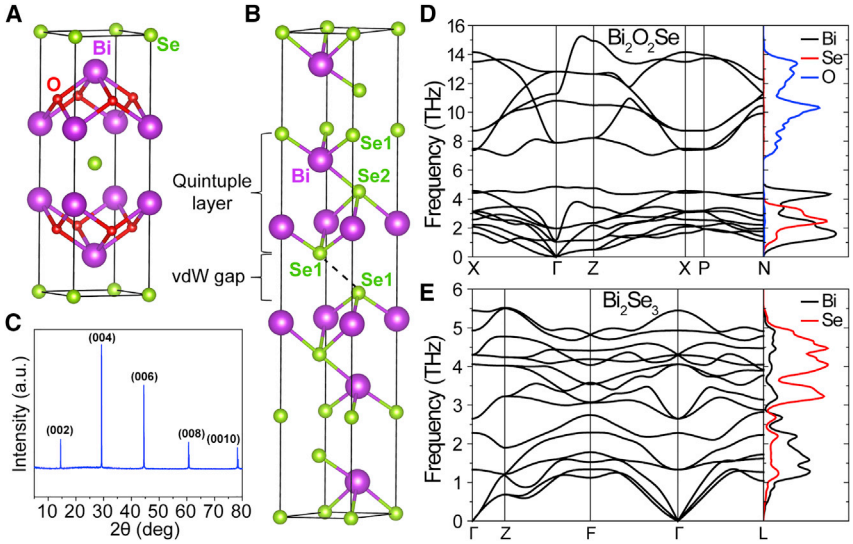

Figure 1. Crystal structure and lattice dynamics

(A and B) Layered crystal structures of (A) Bi_2O_2Se and (B) Bi_2Se_3. Compared with the van der Waals interactions in Bi_2Se_3, a relatively stronger electrostatic force couples the alternating layers in Bi_2O_2Se.

(C) XRD pattern of a Bi_2O_2Se single crystal at 300 K. The characteristic peaks correspond to (002), (004), (006), (008), and (0010) lattice planes of Bi_2O_2Se, indicating the pure phase of layered Bi_2O_2Se.

(D and E) Phonon dispersion and DOS of (D) Bi_2O_2Se and (E) Bi_2Se_3.

as shown in Figures 1D and 1E. Compared with Bi_2Se_3, Bi_2O_2Se exhibits pronounced phonon hardening. Substitution of Se by lighter O results in a maximum frequency of 15.3 THz in Bi_2O_2Se, much higher than that (5.5 THz) in Bi_2Se_3. A phonon bandgap of 2.1 THz arises in Bi_2O_2Se because of the large mass difference between O and the other two elements. Despite the same atomic mass, the vibrational spectra of Bi atoms differ a lot between the two materials. Similarly, Se atoms in the two materials possess different vibrational spectra. In Bi_2O_2Se, the partial DOS of Bi exhibits two peaks at 4.35 and 1.60 THz, and that of Se is sandwiched in between with a peak at 2.44 THz. In contrast, the phonon DOS of Bi_2Se_3 below and above 2.87 THz are mainly contributed by the vibrations of Bi and Se atoms, respectively.

A similar feature is that both materials possess relatively flat optical branches in the Γ-Z direction compared with the Γ-X direction, which suggests strong anisotropy of group velocity. This feature has been commonly observed in layered materials. In contrast, the anisotropy of acoustic branches along the Γ-Z and Γ-X directions is less significant for each material, as indicated by the sound velocities (Table 1). Compared with Bi_2Se_3, Bi_2O_2Se has relatively more dispersive phonon branches along the Γ-Z direction (for instance, the maximum acoustic phonon frequency along the Γ-Z direction increases from 1.2 THz in Bi_2Se_3 to 2.2 THz in Bi_2O_2Se), resulting in higher group velocities and consequently higher through-plane thermal conductivity. Specifically, the sound velocity of the LA branch in Bi_2O_2Se is 1.8 times of that in Bi_2Se_3, as shown in Table 1. The higher through-plane thermal conductivity in Bi_2O_2Se will be confirmed by our TDTR measurements and *ab initio* phonon transport calculations.

Thermal conductivity measurements and calculations

We measured the through-plane thermal conductivities κ_z of both materials using TDTR. Bulk Bi_2O_2Se single crystalline samples were synthesized using a modified

Please cite this article in press as: Guo et al., Electrostatic interaction determines thermal conductivity anisotropy of Bi_2O_2Se, Cell Reports Physical Science (2021), https://doi.org/10.1016/j.xcrp.2021.100624

Table 1. Sound velocities of acoustic branches (TA1, TA2, and LA) along the Γ-Z and Γ-X directions for Bi_2O_2Se and Bi_2Se_3

Group velocity (km s^{-1})		Bi_2O_2Se	Bi_2Se_3
Γ-Z (through plane)	TA1	1.27	1.81
	TA2	1.21	1.80
	LA	3.94	2.21
Γ-X (in plane)	TA1	1.10	1.45
	TA2	2.63	1.76
	LA	4.33	2.54

Bridgman method.[1] Details of our sample preparation are presented in Experimental procedures. The single-crystalline nature of the as-synthesized sample was confirmed by X-ray diffraction (XRD) characterization, as shown in Figure 1C. Single-crystalline Bi_2Se_3 samples were purchased directly from 2Dsemiconductors USA. The Bi_2O_2Se and Bi_2Se_3 samples are bulk crystals with a lateral size of 5–10 mm and a thickness of tens of micrometers. The in-plane κ_r and through-plane thermal conductivities κ_z are calculated by the *ab initio* phonon Boltzmann transport approach. Details of the thermal characterization and *ab initio* calculations can be found in Experimental procedures.

Figure 2 summarizes the measured and calculated thermal conductivity of single-crystalline Bi_2O_2Se and Bi_2Se_3 samples as a function of temperature. Our measurements and *ab initio* calculations show that the through-plane thermal conductivity κ_z of Bi_2O_2Se is relatively higher than that of Bi_2Se_3 over a temperature range of 80–300 K. Above 200 K, the measured κ_z values of both materials agree well with the *ab initio* calculations. For instance, at room temperature, the TDTR measurements give 0.86 $\pm$ 0.09 W m^{-1} K^{-1} for Bi_2O_2Se and 0.81 $\pm$ 0.12 W m^{-1} K^{-1} for Bi_2Se_3, whereas the *ab initio* method predicts 0.92 and 0.70 W m^{-1} K^{-1} for the naturally occurring forms of Bi_2O_2Se and Bi_2Se_3, respectively. Our measured κ_z value of Bi_2Se_3 is close to the value of 0.82 $\pm$ 0.18 W m^{-1} K^{-1} reported by Fournier et al.[25] As the temperature decreases, the measured and calculated κ_z values increase because the intrinsic phonon-phonon scattering becomes weaker, whereas the measurements exhibit a weaker temperature dependence when the temperature is below 200 K. This discrepancy is likely due to extrinsic scatterings by the inevitable defects in the measured samples, which are temperature independent and become relatively stronger at lower temperatures. Similar discrepancies between the measurements and theoretical calculations of the through-plane thermal conductivity have also been observed in some other layered materials, such as MoS_2, WS_2, and hexagonal boron nitride.[26,27]

In contrast to the through-plane thermal conductivity where Bi_2O_2Se has a higher κ_z than Bi_2Se_3, our *ab initio* phonon transport calculations show that the in-plane thermal conductivity κ_r of Bi_2O_2Se is around 30% lower than that of Bi_2Se_3 over the entire measured temperature range of 80–300 K. The κ_r of Bi_2O_2Se is predicted to be 1.85 W m^{-1} K^{-1} at 300 K, which is close to that measured by Yang et al.[29] (1.91 $\pm$ 0.24 W m^{-1} K^{-1}) for a 40-nm-thick single-crystalline film sample. Our calculations show that the κ_r of the 40-nm-thick sample already reaches 92% of the bulk κ_r because of its short mean free paths. More details regarding the thickness dependence of κ_z and κ_r are presented in the subsequent discussion. Previously measured thermal conductivity of polycrystalline Bi_2O_2Se mostly ranges from 0.9–1.7 W m^{-1} K^{-1} at 300 K, lying between our κ_z and κ_r results, which is expected considering its thermal anisotropy and weak boundary scattering because of the short mean free paths. The κ_r of Bi_2Se_3 is predicted to be 2.50 W m^{-1} K^{-1} at 300 K, agreeing well

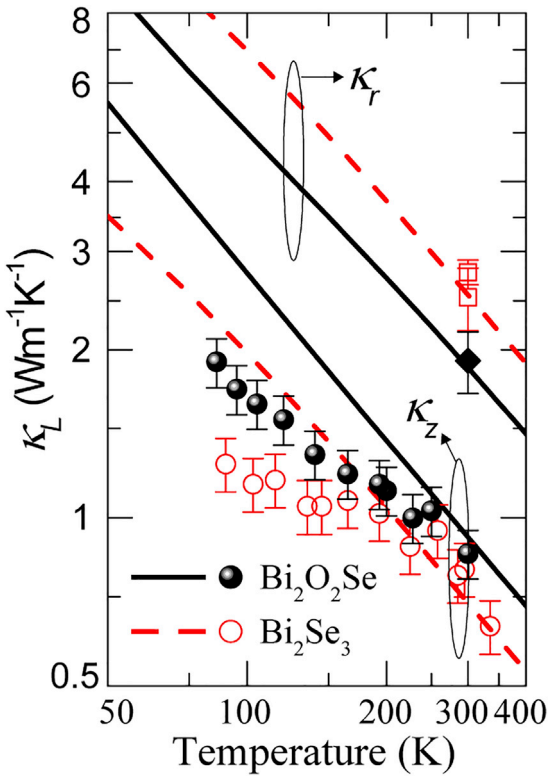

Figure 2. In-plane and through-plane thermal conductivity of Bi_2O_2Se and Bi_2Se_3 single crystals as a function of temperature

The circles represent the current measurements of κ_z for Bi_2O_2Se (solid) and Bi_2Se_3 (open) using TDTR, and the curves are the predictions of κ_z and κ_r for Bi_2O_2Se (solid) and Bi_2Se_3 (dashed) from the *ab initio* phonon Boltzmann transport calculations. For comparison, the measured κ_r of Bi_2O_2Se by Qian et al.[28] (solid diamond) and Bi_2Se_3 by Yang et al.[29] (open squares) are also plotted. The error bars represent the measurement uncertainties estimated using the error propagation formula, taking into account all uncertainties of the input parameters.

with the measurements by Qian et al.[28] (2.75 $\pm$ 0.14 W m^{-1} K^{-1} and 2.48 $\pm$ 0.32 W m^{-1} K^{-1}) for undoped Bi_2Se_3. We note that relatively higher values were measured by Fournier et al.[25] (3.5 $\pm$ 0.35 W m^{-1} K^{-1}) and Navrátil[30] (3.10 W m^{-1} K^{-1}). This discrepancy is probably due to the contribution of electronic carriers in these measurements because their samples were *n* doped with a high carrier concentration on the order of 10^{19} cm^{-3}. In contrast, our Bi_2Se_3 samples are unintentionally light doped with a low carrier concentration on the order of 10^{17} cm^{-3}.

The higher κ_z but lower κ_r in Bi_2O_2Se results in substantially smaller thermal anisotropy (defined as κ_r/κ_z) than that in Bi_2Se_3. For instance, the calculated thermal anisotropy of Bi_2O_2Se is 2.0, whereas that of Bi_2Se_3 is 3.6 at 300 K. We note that previous *ab initio* calculations predict quite scattered values of thermal anisotropy (from 1.6 to ~6 at 300 K) for Bi_2O_2Se, although they all used the generalized gradient approximation (GGA) for the exchange-correlation functional.[31–33] Many previous studies have shown that GGA is inappropriate for layered materials because it often underestimates lattice thermal conductivity because of the underestimation of bonding strength.[34–36] We instead used the local density approximation (LDA) for the exchange-correlation functional, which has been demonstrated to be more accurate in predicting the thermal conductivity of layered materials such as Bi_2Te_3, SnSe, and $HfTe_5$.[35,37,38]

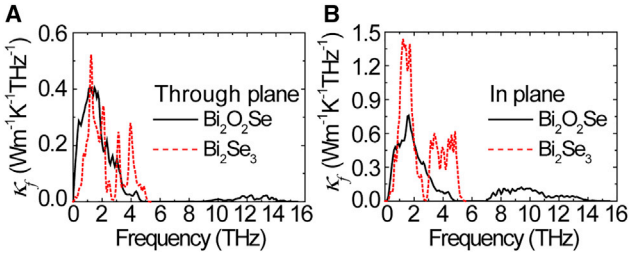

Figure 3. Phonon spectral contribution of thermal conductivity κ_f

(A and B) κ_f of Bi_2O_2Se and Bi_2Se_3 as a function of phonon frequency along the (A) through-plane and (B) in-plane directions at 300 K. The different thermal anisotropy of the two materials is mainly determined by phonons below 5 THz, which contribute the most to the κ_z and κ_r of both materials.

Analysis on anisotropic thermal conductivity

We now look into the spectral thermal conductivity along the through-plane and in-plane directions to understand the smaller thermal anisotropy in Bi_2O_2Se in comparison with Bi_2Se_3. As shown in Figure 3, the κ_z and κ_r of both materials at 300 K are mainly contributed by phonons below 5 THz, although phonons in the range of 7–14 THz also contribute to the thermal conductivity in Bi_2O_2Se. Along the through-plane direction, the overall contribution of phonons below 5 THz is comparable between the two materials. However, Bi_2O_2Se phonons have notably more contribution below 1 THz but less in the range of 3.5–5 THz. Along the in-plane direction, phonons in the range of 1–2 and 3–5 THz have substantially smaller contributions in Bi_2O_2Se compared with Bi_2Se_3.

The spectral thermal conductivity contribution is determined by phonon lifetime, group velocity, and specific heat. Because these two materials have a similar specific heat below 5 THz (only 7.5% lower in Bi_2O_2Se according to our calculation), the difference in spectral thermal conductivity must be mainly due to the phonon lifetimes and/or the group velocities. Compared with Bi_2Se_3, Bi_2O_2Se has substantially shorter phonon lifetimes in most of the frequency range, as shown in Figure 4A. However, the larger through-plane component of the group velocity of many phonon modes below 4 THz in Bi_2O_2Se (Figure 4B) compensates for its shorter lifetime, producing comparable spectral thermal conductivity along the through-plane direction between the two materials. In contrast, both materials have similar in-plane components of the group velocity in the range of 1–2 and 3–5 THz (Figure 4c), resulting in lower spectral thermal conductivity in Bi_2O_2Se.

Figures 4B and 4C show that the group velocity ratio v_z/v_x of many modes is remarkably larger in Bi_2O_2Se than in Bi_2Se_3, implying that phonon focusing in Bi_2O_2Se should be much weaker than that in Bi_2Se_3. The phonon focusing effect is typically evaluated by phonon isoenergy surfaces. Because the group velocity vector is perpendicular to the isoenergy surface, the anisotropy of isoenergy surfaces can be directly related to the anisotropy of the thermal conductivity tensor. The isoenergy surfaces of three acoustic phonon branches in both materials are shown in Figure 5. Both materials have typical features of isoenergy surfaces of layered materials; namely, approaching a circular shape near the Brillouin zone center while becoming more flattened near the zone edges, similar to what has been observed for transition metal dichalcogenides.[24] However, many isoenergy surfaces in Bi_2O_2Se have a larger curvature than those in Bi_2Se_3 in the frequency range of 0.6–2.0 THz for each acoustic branch, resulting in a larger fraction of the group velocity component along the through-plane direction. For example, the 1.6-THz isoenergy surface of the LA branch (below which is filled by yellow) is almost flat for Bi_2Se_3 but markedly curved for Bi_2O_2Se.

Please cite this article in press as: Guo et al., Electrostatic interaction determines thermal conductivity anisotropy of Bi_2O_2Se, Cell Reports Physical Science (2021), https://doi.org/10.1016/j.xcrp.2021.100624

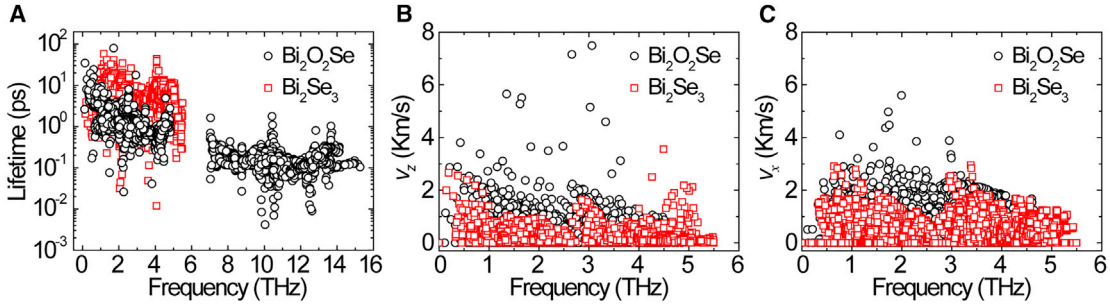

Figure 4. Phonon modal properties

(A–C) Phonon modal lifetime at 300 K (A), *z* (through-plane, B), and *x* (in-plane, C) components of group velocity for Bi_2O_2Se and Bi_2Se_3. Compared with Bi_2Se_3, Bi_2O_2Se exhibits a remarkably larger group velocity ratio v_z/v_x for many phonon modes, implying a weaker phonon focusing effect.

We now seek the physical mechanisms of the enhanced curvature of the isoenergy surfaces in Bi_2O_2Se. Substitution of Se by O induces a change in atomic mass and bonding strength. The lighter atomic mass causes similar phonon hardening along both the through-plane and in-plane directions, causing no change in the anisotropy of group velocities or isoenergy surfaces. We then calculated the elastic constants of both materials, obtaining C_{11} = 159.1 (in plane) and C_{33} = 121.1 GPa (through plane) for Bi_2O_2Se and C_{11} = 98.3 and C_{33} = 60.1 GPa for Bi_2Se_3. Indeed, the elastic anisotropy decreases from 1.6 in Bi_2Se_3 to 1.3 in Bi_2O_2Se, leading to more isotropic isoenergy surfaces. The overwhelming enhancement of C_{33} versus C_{11} in Bi_2O_2Se comes from the electrostatic interactions along the through-plane direction, which is markedly stronger than the van der Waals interactions in Bi_2Se_3. Specifically, the interlayer Bi-Se bond strength (0.84 eV/Å^2) in Bi_2O_2Se is much stronger than that of Se1-Se1 (0.29 eV/Å^2) and Bi-Se2 (0.73 eV/Å^2) interactions in Bi_2Se_3 (Figures 1A and 1B for different bonds). The stronger interlayer interaction in Bi_2O_2Se induces phonon hardening in the Γ-Z direction. Consider that the maximum acoustic frequency in the Γ-Z direction in Bi_2O_2Se has increased by 83.3% compared with that in Bi_2Se_3, of which the 23.8% mass decrease from Bi_2Se_3 to Bi_2O_2Se contributes only 11.4% (assuming the single atomic chain model, we have $\omega = \sqrt{K/m}$, where *K* is the force constant and *m* is the mass), all the rest of the frequency increase is likely contributed by the stronger interlayer Bi-Se bonding in Bi_2O_2Se.

Thickness dependence of thermal conductivity

Special attention has been paid to the thin films of Bi_2O_2Se mainly because of the unique thickness dependence of electronic properties, such as the high mobility in the 6.7-nm thickness single crystal.[1] Therefore, we calculate the thickness-dependent κ_z and κ_r of Bi_2O_2Se at 300 K and compared them with Bi_2Se_3, as shown in Figure 6A. Overall, the thermal conductivity of both materials has a very weak thickness dependence along the through-plane and in-plane directions because of their short intrinsic phonon mean free paths. Reducing the thickness to 100 nm causes only 9.0% and 2.1% reduction in κ_z and κ_r of Bi_2O_2Se, respectively. The κ_r in Bi_2O_2Se possesses a weaker thickness dependence than that in Bi_2Se_3; e.g., 6.4% versus 15.1% reduction of κ_r for a 20-nm-thick film compared with the bulk. This is due to the shorter mean free paths in Bi_2O_2Se, as shown in Figure 6B. Specifically, the cumulative κ_r reaches 90% of the total thermal conductivity at 10 and 17 nm for Bi_2O_2Se and Bi_2Se_3, respectively. The calculated κ_r of Bi_2O_2Se agrees favorably with the measurements by Yang et al.[29] for thick samples, whereas the discrepancy is larger for the films thinner than 20 nm. This may be due to the increasing contribution of ballistic transport to heat conduction, which can result in underestimated thermal conductivity in Raman measurements, where diffusive transport is assumed when extracting

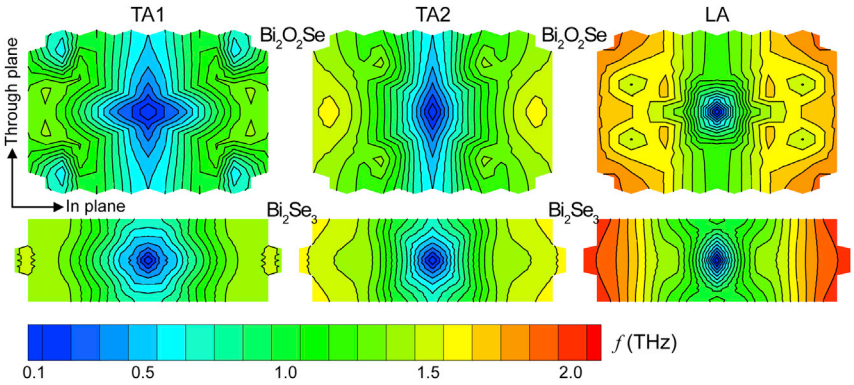

Figure 5. Anisotropy analysis of phonon isoenergy surfaces

Isoenergy surfaces of two transverse (TA1 and TA2) and longitudinal (LA) acoustic phonon branches for Bi_2O_2Se (Z-Γ-X plane, top) and Bi_2Se_3 (Z-Γ-L plane, bottom). The color scale bar at the bottom indicates the magnitudes of phonon frequencies. The comparison of isoenergy surfaces indicates weaker phonon focusing of acoustic branches (particularly for the frequency range 0.6–2.0 THz) in Bi_2O_2Se.

the thermal conductivity values.[39] Along the through-plane direction, the κ_z of both materials shows a similar thickness dependence. The cumulative κ_z saturates at a similarly short mean free path (around 20 nm) for both materials.

In summary, we combined TDTR measurements and *ab initio* phonon transport calculations to study the anisotropic thermal conductivity of Bi_2O_2Se over a temperature range of 80–300 K in comparison with Bi_2Se_3. The thermal conductivity of Bi_2O_2Se is relatively higher along the through-plane direction but lower along the in-plane direction, resulting in much smaller thermal anisotropy. This behavior originates from the reduced anisotropy of phonon isoenergy surfaces, producing weakened phonon focusing in the in-plane directions. Essentially, the modification of isoenergy surfaces is mainly due to the enhanced interlayer bonding strength induced by the stronger electrostatic interaction than the typical van der Waals interaction. This fundamental understanding offers new insights into the origin of thermal anisotropy in layered materials. The thermal conductivity (temperature and thickness dependence) and spectral phonon transport details presented in this work will help practical thermal engineering for Bi_2O_2Se-based electronics and thermoelectrics.

EXPERIMENTAL PROCEDURES

Resource availability

Lead contact

Further information and requests for resources should be directed to and will be fulfilled by the lead contact, Ronggui Yang (ronggui@hust.edu.cn).

Materials availability

This study did not generate new unique reagents.

Data and code availability

All data are available from the lead contact upon reasonable request.

Sample preparation

Bi_2O_2Se single crystals were synthesized in Peng's lab at Peking University using a modified Bridgman method. Stoichiometric high-purity Bi_2O_3 powder (Alfa Aesar, 5 N) and Bi_2Se_3 powder (Alfa Aesar, 5 N) were mixed and put into an evacuated

Please cite this article in press as: Guo et al., Electrostatic interaction determines thermal conductivity anisotropy of Bi_2O_2Se, Cell Reports Physical Science (2021), https://doi.org/10.1016/j.xcrp.2021.100624

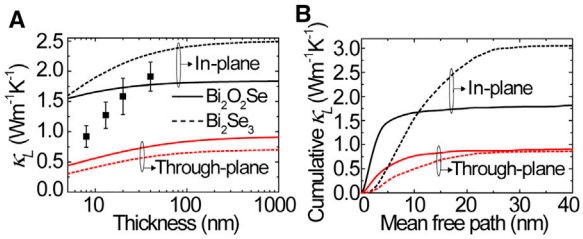

Figure 6. Thickness dependence of thermal conductivity

(A) Thermal conductivity of Bi_2O_2Se and Bi_2Se_3 as a function of film thickness.

(B) Cumulative thermal conductivity versus mean free path. The curves represent the predicted results of Bi_2O_2Se (solid) and Bi_2Se_3 (dashed) from the *ab initio* phonon Boltzmann transport calculations in comparison with the thickness-dependent κ_r of Bi_2O_2Se measured by Yang et al.[29] (symbols), with the error bars showing the measurement uncertainties.

quartz tube with pressure down to 10^{-2} Pa. Bi_2O_2Se powder was first synthesized by maintaining the temperature at 873 K for 12 h. After being ground adequately, the as-synthesized Bi_2O_2Se powder was put into an evacuated quartz tube again. Bi_2O_2Se single crystals were obtained by melting Bi_2O_2Se powder at 1,223 K for 5 min, slowly cooling down to 1,163 K over 9 h, and finally cooling to room temperature.

The single-crystalline Bi_2Se_3 samples were purchased directly from 2Dsemiconductors USA. These Bi_2Se_3 samples were doped unintentionally with an impurity concentration on the order of 10^{17} cm^{-3}. The electronic contribution to the thermal conductivity of the crystals should be negligibly small with such low carrier concentrations.

Thermal conductivity characterization

The through-plane thermal conductivities of Bi_2O_2Se and Bi_2Se_3 were measured using TDTR at different temperatures in the range of 80–300 K. With this method,[40] a train of femtosecond laser pulses modulated at a frequency between 1–10 MHz was used to induce heating events on the sample surface; another train of delayed laser pulses detected the surface temperature change via thermoreflectance as a function of the delay time. A 100-nm-thick Al transducer layer was deposited on the sample surface for TDTR measurements. The through-plane thermal conductivity of the sample κ_z and the Al/sample interface thermal conductance G could be extracted by comparing the measured signal with a thermal model calculation. A relatively large laser spot size ($1/e^2$ radius) of 10 μm was used for the measurements. The laser power was chosen carefully to make sure that the measurements do not depend on the laser power; see Note S1 for more details. Unlike TDTR measurements of some other layered materials, like MoS_2,[26] no obvious modulation frequency dependence was observed in the measurements of Bi_2O_2Se and Bi_2Se_3 (Figure S1). The in-plane thermal conductivity was not measured here because of the lack of sensitivity. Typically, the TDTR technique could reliably measure $\kappa_r < 10$ W m^{-1} K^{-1} with an uncertainty of less than 30%.[41] The uncertainty could be larger than 100% when κ_r is around 1 W m^{-1} K^{-1}.

Ab initio lattice thermal conductivity calculation

The lattice thermal conductivity was calculated by iteratively solving the linearized Peierls-Boltzmann transport equation. The phonon dispersion was determined by diagonalizing the dynamic matrix constructed from the second-order interatomic force constants (IFCs). The phonon relaxation time of bulk crystals was calculated by considering phonon-phonon scattering determined by third-order IFCs and phonon-isotope scattering terms based on the Matthiessen rule. The isotopes

were assumed as occurring naturally. Phonon boundary scattering was included for thin films. A 19 × 19 × 19 **q**-mesh was used to calculate the lattice thermal conductivity, and the tetrahedron method was employed for energy conservation. More technical details can be found in previous publications.[36,42–45]

The IFCs were extracted from density functional theory calculations using the projector augmented wave method,[46] as implemented in the Vienna *ab initio* simulation package (VASP).[47] The LDA was used for the exchange-correlation functional. The self-consistent calculation was performed with a cutoff energy of 550 eV for Bi_2O_2Se and 350 eV for Bi_2Se_3 and a force convergence criterion of 10^{-6} eV/Å for both materials. A supercell of 4 × 4 × 4 was used to calculate all IFCs. The spin-orbit interaction was included.

Recent studies show that phonon renormalization and four-phonon scattering are important for predicting the thermal properties of materials such as PbTe, particularly at high temperatures.[48–52] Unfortunately, the four-phonon scattering calculation is currently prohibitively costly for Bi_2O_2Se and Bi_2Se_3 because of their large unit cells. Here we obtained good agreement between calculations and experiments for the thermal conductivity of Bi_2O_2Se, implying that phonon renormalization and four-phonon scattering may have a minor effect on the thermal conductivity calculation. One possible reason is that the four-phonon scattering is not strongly excited in the temperature range considered in this study. However, this postulation is not conclusive, and the agreement could also be due to coincidence. Specifically, the enhancement of total scattering rates by four-phonon scattering can be mostly canceled out by the decrease of three-phonon scattering rates because of anharmonic phonon renormalization, coincidentally resulting in similar thermal conductivity values predicted in the framework of three-phonon scattering and harmonic approximation. This cancellation effect has been observed for prediction of PbTe[51] and NaCl.[52]

SUPPLEMENTAL INFORMATION

Supplemental information can be found online at https://doi.org/10.1016/j.xcrp.2021.100624.

ACKNOWLEDGMENTS

We acknowledge support from the National Natural Science Foundation of China (21733001 and 21920102004) and the National Basic Research Program of China (2016YFA0200101). This work used the research computing facilities at Shandong Institute of Advanced Technology and the Linux clusters of the Center for Research Computing at the University of Pittsburgh.

AUTHOR CONTRIBUTIONS

R.Y., R.G., and P.J. conceived the idea. R.G. performed the simulations. P.J. conducted the experiments. T.T. prepared the materials. All authors contributed to the analyses, discussions, and writing of the manuscript.

DECLARATION OF INTERESTS

The authors declare no competing interests.

Received: July 20, 2021
Revised: September 7, 2021
Accepted: October 5, 2021
Published: October 22, 2021

REFERENCES

1. Wu, J., Yuan, H., Meng, M., Chen, C., Sun, Y., Chen, Z., Dang, W., Tan, C., Liu, Y., Yin, J., et al. (2017). High electron mobility and quantum oscillations in non-encapsulated ultrathin semiconducting Bi_2O_2Se. Nat. Nanotechnol. *12*, 530–534.
2. Zhang, C., Wu, J., Sun, Y., Tan, C., Li, T., Tu, T., Zhang, Y., Liang, Y., Zhou, X., Gao, P., and Peng, H. (2020). High-Mobility Flexible Oxyselenide Thin-Film Transistors Prepared by a Solution-Assisted Method. J. Am. Chem. Soc. *142*, 2726–2731.
3. Wu, M., and Zeng, X.C. (2017). Bismuth oxychalcogenides: a new class of ferroelectric/ferroelastic materials with ultra high mobility. Nano Lett. *17*, 6309–6314.
4. Liu, S., Tan, C., He, D., Wang, Y., Peng, H., and Zhao, H. (2020). Optical Properties and Photocarrier Dynamics of Bi_2O_2Se Monolayer and Nanoplates. Adv. Opt. Mater. *8*, 1901567.
5. Pan, L., Zhao, L., Zhang, X., Chen, C., Yao, P., Jiang, C., Shen, X., Lyu, Y., Lu, C., Zhao, L.D., and Wang, Y. (2019). Significant Optimization of Electron-Phonon Transport of n-Type Bi_2O_2Se by Mechanical Manipulation of Se Vacancies via Shear Exfoliation. ACS Appl. Mater. Interfaces *11*, 21603–21609.
6. Ren, G., Lan, J., Zhao, L., Liu, C., Yuan, H., Shi, Y., Zhou, Z., and Lin, Y. (2019). Layered oxygen-containing thermoelectric materials: Mechanisms, strategies, and beyond. Mater. Today *29*, 68–85.
7. Tan, X., Liu, Y., Liu, R., Zhou, Z., Liu, C., Lan, J., Zhang, Q., Lin, Y., and Nan, C. (2019). Synergistical Enhancement of Thermoelectric Properties in *n*-Type Bi_2O_2Se by Carrier Engineering and Hierarchical Microstructure. Adv. Energy Mater. *9*, 1900354.
8. Pan, L., Liu, W., Zhang, J., Shi, X., Gao, H., Liu, Q., Shen, X., Lu, C., Wang, Y., and Chen, Z. (2020). Synergistic effect approaching record-high figure of merit in the shear exfoliated n-type $Bi_2O_{2-2x}Te_{2x}Se$. Nano Energy *69*, 104394.
9. Yang, F., Wu, J., Suwardi, A., Zhao, Y., Liang, B., Jiang, J., Xu, J., Chi, D., Hippalgaonkar, K., and Lu, J. (2021). Gate-Tunable Polar Optical Phonon to Piezoelectric Scattering in Few-Layer Bi_2O_2Se for High-Performance Thermoelectrics. Adv. Mater. *33*, 2004786.
10. Li, H., Xu, X., Zhang, Y., Gillen, R., Shi, L., and Robertson, J. (2018). Native point defects of semiconducting layered Bi_2O_2Se. Sci. Rep. *8*, 10920.
11. Huang, X., Niu, C., Zhang, J., Wang, A., Jia, Y., and Song, Y. (2019). Strain-tunable electronic structure, optical response, and high electron mobility of Bi_2O_2Se crystals. APL Mater. *7*, 081110.
12. Chen, C., Wang, M., Wu, J., Fu, H., Yang, H., Tian, Z., Tu, T., Peng, H., Sun, Y., Xu, X., et al. (2018). Electronic structures and unusually robust bandgap in an ultrahigh-mobility layered oxide semiconductor, Bi_2O_2Se. Sci. Adv. *4*, eaat8355.
13. Ruleova, P., Drasar, C., Lostak, P., Li, C., Ballikaya, S., and Uher, C. (2010). Thermoelectric properties of Bi_2O_2Se. Mater. Chem. Phys. *119*, 299–302.
14. Zhang, K., Hu, C., Kang, X., Wang, S., Xi, Y., and Liu, H. (2013). Synthesis and thermoelectric properties of Bi_2O_2Se nanosheets. Mater. Res. Bull. *48*, 3968–3972.
15. Zhan, B., Liu, Y., Tan, X., Lan, J., Lin, Y., and Nan, C. (2015). Enhanced thermoelectric properties of Bi_2O_2Se ceramics by Bi deficiencies. J. Am. Ceram. Soc. *98*, 2465–2469.
16. Tan, X., Lan, J., Ren, G., Liu, Y., Lin, Y., and Nan, C. (2017). Enhanced thermoelectric performance of *n*-type Bi_2O_2Se by Cl-doping at Se site. J. Am. Ceram. Soc. *100*, 1494–1501.
17. Tan, X., Lan, J., Hu, K., Xu, B., Liu, Y., Zhang, P., Cao, X., Zhu, Y., Xu, W., and Lin, Y. (2018). Boosting the thermoelectric performance of Bi_2O_2Se by isovalent doping. J. Am. Ceram. Soc. *101*, 4634–4644.
18. Pan, L., Zhang, J., Chen, C., and Wang, Y. (2020). Enhanced thermoelectric properties of highly textured $Bi_2O_{2-x}Se_{1+x}$ with liquid-phase mechanical exfoliation. Scr. Mater. *178*, 376–381.
19. Gibson, Q.D., Zhao, T., Daniels, L.M., Walker, H.C., Daou, R., Hébert, S., Zanella, M., Dyer, M.S., Claridge, J.B., and Slater, B. (2021). Low thermal conductivity in a modular inorganic material with bonding anisotropy and mismatch. Science *373*, 1017–1022.
20. Touloukian, Y.S. (1970). Thermophysical properties of matter: Thermal Conductivity: Nonmetallic Solids (IFI/Plenum).
21. Zhao, L.D., Lo, S.H., Zhang, Y., Sun, H., Tan, G., Uher, C., Wolverton, C., Dravid, V.P., and Kanatzidis, M.G. (2014). Ultralow thermal conductivity and high thermoelectric figure of merit in SnSe crystals. Nature *508*, 373–377.
22. Minnich, A. (2015). Phonon heat conduction in layered anisotropic crystals. Phys. Rev. B Condens. Matter Mater. Phys. *91*, 085206.
23. Chen, Z., and Dames, C. (2015). An anisotropic model for the minimum thermal conductivity. Appl. Phys. Lett. *107*, 193104.
24. Guo, R., Jho, Y.D., and Minnich, A.J. (2018). Coherent control of thermal phonon transport in van der Waals superlattices. Nanoscale *10*, 14432–14440.
25. Fournier, D., Marangolo, M., Eddrief, M., Kolesnikov, N.N., and Frétigny, C. (2018). Straightforward measurement of anisotropic thermal properties of a Bi_2Se_3 single crystal. J. Phys. Condens. Matter *30*, 115701.
26. Jiang, P., Qian, X., Gu, X., and Yang, R. (2017). Probing Anisotropic Thermal Conductivity of Transition Metal Dichalcogenides MX_2 (M = Mo, W and X = S, Se) using Time-Domain Thermoreflectance. Adv. Mater. *29*, 1701068.
27. Jiang, P., Qian, X., Yang, R., and Lindsay, L. (2018). Anisotropic thermal transport in bulk hexagonal boron nitride. Phys. Rev. Mater. *2*, 064005.
28. Qian, X., Ding, Z., Shin, J., Schmidt, A.J., and Chen, G. (2020). Accurate measurement of in-plane thermal conductivity of layered materials without metal film transducer using frequency domain thermoreflectance. Rev. Sci. Instrum. *91*, 064903.
29. Yang, F., Wang, R., Zhao, W., Jiang, J., Wei, X., Zheng, T., Yang, Y., Wang, X., Lu, J., and Ni, Z. (2019). Thermal transport and energy dissipation in two-dimensional Bi_2O_2Se. Appl. Phys. Lett. *115*, 193103.
30. Navrátil, J., Horák, J., Plecháček, T., Kamba, S., Lošťák, P., Dyck, J., Chen, W., and Uher, C. (2004). Conduction band splitting and transport properties of Bi_2Se_3. J. Solid State Chem. *177*, 1704–1712.
31. Wang, C., Ding, G., Wu, X., Wei, S., and Gao, G. (2018). Electron and phonon transport properties of layered Bi_2O_2Se and Bi_2O_2Te from first-principles calculations. New J. Phys. *20*, 123014.
32. Song, H.Y., Ge, X.J., Shang, M.Y., Zhang, J., and Lü, J.T. (2019). Intrinsically low thermal conductivity of bismuth oxychalcogenides originating from interlayer coupling. Phys. Chem. Chem. Phys. *21*, 18259–18264.
33. Zhu, X.L., Liu, P.F., Xie, G., and Wang, B.T. (2019). First-principles study of thermal transport properties in the two- and three-dimensional forms of Bi_2O_2Se. Phys. Chem. Chem. Phys. *21*, 10931–10938.
34. Linnera, J., and Karttunen, A. (2017). Ab initio study of the lattice thermal conductivity of Cu_2O using the generalized gradient approximation and hybrid density functional methods. Phys. Rev. B *96*, 014304.
35. Feng, T., Wu, X., Yang, X., Wang, P., Zhang, L., Du, X., Wang, X., and Pantelides, S.T. (2019). Thermal Conductivity of $HfTe_5$: A Critical Revisit. Adv. Funct. Mater. *30*, 1907286.
36. Guo, R., Wang, X., and Huang, B. (2015). Thermal conductivity of skutterudite $CoSb_3$ from first principles: Substitution and nanoengineering effects. Sci. Rep. *5*, 7806.
37. Hellman, O., and Broido, D.A. (2014). Phonon thermal transport in Bi_2Te_3 from first principles. Phys. Rev. B Condens. Matter Mater. Phys. *90*, 134309.
38. Guo, R., Wang, X., Kuang, Y., and Huang, B. (2015). First-principles study of anisotropic thermoelectric transport properties of IV-VI semiconductor compounds SnSe and SnS. Phys. Rev. B Condens. Matter Mater. Phys. *92*, 115202.
39. Chen, S., Moore, A.L., Cai, W., Suk, J.W., An, J., Mishra, C., Amos, C., Magnuson, C.W., Kang, J., Shi, L., and Ruoff, R.S. (2011). Raman measurements of thermal transport in suspended monolayer graphene of variable sizes in vacuum and gaseous environments. ACS Nano *5*, 321–328.
40. Jiang, P., Qian, X., and Yang, R. (2018). Tutorial: Time-domain thermoreflectance (TDTR) for thermal property characterization of bulk and thin film materials. J. Appl. Physiol. *124*, 161103.
41. Jiang, P., Qian, X., and Yang, R. (2017). Time-domain thermoreflectance (TDTR) measurements of anisotropic thermal conductivity using a variable spot size approach. Rev. Sci. Instrum. *88*, 074901.

42. Broido, D.A., Malorny, M., Birner, G., Mingo, N., and Stewart, D.A. (2007). Intrinsic lattice thermal conductivity of semiconductors from first principles. Appl. Phys. Lett. *91*, 231922.

43. Ward, A., Broido, D., Stewart, D.A., and Deinzer, G. (2009). Ab initio theory of the lattice thermal conductivity in diamond. Phys. Rev. B Condens. Matter Mater. Phys. *80*, 125203.

44. Lindsay, L., Broido, D.A., and Reinecke, T.L. (2012). Thermal conductivity and large isotope effect in GaN from first principles. Phys. Rev. Lett. *109*, 095901.

45. Li, W., Carrete, J., Katcho, N.A., and Mingo, N. (2014). ShengBTE: A solver of the Boltzmann transport equation for phonons. Comput. Phys. Commun. *185*, 1747–1758.

46. Blöchl, P.E. (1994). Projector augmented-wave method. Phys. Rev. B Condens. Matter *50*, 17953–17979.

47. Kresse, G., and Furthmüller, J. (1996). Efficient iterative schemes for ab initio total-energy calculations using a plane-wave basis set. Phys. Rev. B Condens. Matter *54*, 11169–11186.

48. Romero, A., Gross, E., Verstraete, M., and Hellman, O. (2015). Thermal conductivity in PbTe from first principles. Phys. Rev. B Condens. Matter Mater. Phys. *91*, 214310.

49. Lu, Y., Sun, T., and Zhang, D. (2018). Lattice anharmonicity, phonon dispersion, and thermal conductivity of PbTe studied by the phonon quasiparticle approach. Phys. Rev. B *97*, 174304.

50. Ribeiro, G.A., Paulatto, L., Bianco, R., Errea, I., Mauri, F., and Calandra, M. (2018). Strong anharmonicity in the phonon spectra of PbTe and SnTe from first principles. Phys. Rev. B *97*, 014306.

51. Xia, Y. (2018). Revisiting lattice thermal transport in PbTe: The crucial role of quartic anharmonicity. Appl. Phys. Lett. *113*, 073901.

52. Ravichandran, N.K., and Broido, D. (2018). Unified first-principles theory of thermal properties of insulators. Phys. Rev. B *98*, 085205.